1 **Title**

2 **Pyrimidine starvation activates a bistable phenotypic switch leading to ribosome provisioning and**
3 **rapid exit from stationary phase**

4

5 **Authors:**

6 P. Remigi[1], G.C. Ferguson[2], S. De Monte[3] and P.B. Rainey[1,4,5]

7 [1] New Zealand Institute for Advanced Study, Massey University, Auckland 0745, New Zealand

8 [2] Institute of Natural and Mathematical Sciences, Massey University, Auckland 0745, New Zealand

9 [3] Institut de Biologie de l'Ecole Normale Superieure, UMR CNRS 8197 INSERM 1024, F-75005 Paris,
10 France

11 [4] Department of Microbial Population Biology, Max Planck Institute for Evolutionary Biology, Plön
12 24306, Germany

13 [5] Ecole Superieure de Physique et de Chimie Industrielles de la Ville de Paris (ESPCI Paris Tech), CNRS
14 UMR 8231, PSL Research University, 75231 Paris, France

15

16 **Corresponding authors:**

17 Philippe Remigi (p.remigi@massey.ac.nz) and Paul B. Rainey (rainey@evolbio.mpg.de)

18

Abstract:

Observations of bacteria at the single-cell level have revealed many instances of phenotypic heterogeneity within otherwise clonal populations, but the selective causes, molecular bases and broader ecological relevance remain poorly understood. In an earlier experiment in which the bacterium *Pseudomonas fluorescens* SBW25 was propagated under a selective regime that mimicked the host immune response, a genotype evolved that stochastically switched between capsulation states. The genetic cause was a mutation in *carB* that decreased the pyrimidine pool (and growth rate) lowering the activation threshold of a pre-existing but hitherto unrecognised phenotypic switch. Genetic components surrounding bifurcation of UTP flux towards DNA/RNA or UDP-glucose (a precursor of colanic acid forming the capsules) were implicated as key components. Extending these molecular analyses – and based on a combination of genetics, transcriptomics, biochemistry and mathematical modelling – we show that pyrimidine limitation triggers an increase in ribosome biosynthesis and that switching is caused by competition between ribosomes and CsrA/RsmA proteins for the mRNA transcript of a feed-forward regulator of colanic acid biosynthesis. We additionally show that in the ancestral bacterium the switch is part of a programme that determines stochastic entry into the semi-quiescent capsulated state, ensures that such cells are provisioned with excess ribosomes, and enables provisioned cells to exit rapidly from stationary phase under permissive conditions.

Introduction:

Phenotypic variation between isogenic cells growing in homogeneous environments can have adaptive consequences, allowing populations to survive unpredictable environmental changes or promoting interactions between different cell types (ACKERMANN 2015; VAN BOXTEL *et al.* 2017). Natural selection, by means of genetic mutations affecting the integration of stochastic noise within signaling pathways, can fine-tune epigenetic switches (ROTEM *et al.* 2010; FRIDMAN *et al.* 2014; NEW *et al.* 2014; RICHARD AND YVERT 2014; VAN DEN BERGH *et al.* 2016; BODI *et al.* 2017) but the molecular details underpinning the evolution of phenotypic heterogeneity remain poorly understood.

An opportunity to study the genetic bases of the evolution of phenotypic heterogeneity arose from a selection experiment where the capacity to switch between different colony phenotypes evolved *de novo* in the bacterium *Pseudomonas fluorescens* SBW25 (BEAUMONT *et al.* 2009). In this experiment, bacteria were passaged through consecutive cycles comprised of single-cell bottlenecks and negative frequency-dependent selection, a regime mimicking essential features of the adaptive immune system in animals. A strain emerged (1B4) that forms distinct opaque or translucent colonies on agar plates. At the single-cell level, this behaviour reflects an epigenetic switch characterized by the bistable production of an extracellular capsule, resulting in the coexistence of two sub-populations of capsulated (Cap+) or non-capsulated (Cap-) cells. Capsules are made of a colanic acid-like polymer, whose production arises from the activity of the *wcaJ-wzb* locus and requires the precursor UDP-glucose. A mutation in *carB*, a gene involved in *de novo* pyrimidine biosynthesis, is responsible for heterogeneous capsule production via a decrease in intracellular pyrimidine pools (BEAUMONT *et al.* 2009; GALLIE *et al.* 2015). Additionally, the switch between capsulated and uncapsulated cells was shown to function in the ancestral gentoype devoid of the *carB* mutation – the *carB* mutation having altered the threshold at which the switch is activated – and underpins the stochastic entry of cells into a semi-quiescent state.

Here we extend earlier work and present a detailed mechanistic model that explains how the *carB* mutation impacts on capsulation heterogeneity. Central to the model is evidence that ribosome biosynthesis is up-regulated upon pyrimidine limitation and that this favors translation of a positively auto-regulated activator of capsular exopolysaccharide biosynthesis that is otherwise inhibited by CsrA/Rsm proteins. The switch comprises part of a programme that facilitates stochastic entry into a semi-quiescent state and rapid exit from this state upon realisation of permissive conditions through modulation of ribosome levels.

Results

Capsulation is not induced by UDP-glucose depletion

The paradoxical observation that pyrimidine limitation induced capsulation, a phenotypic trait depleting the pyrimidine pool even more through the consumption of UDP-glucose, caused attention to focus on the link between capsulation, growth and pyrimidine metabolism (GALLIE *et al.* 2015). In particular, the fact that capsulation may represent a semi-quiescent state whose initiation is triggered by fluctuations in the concentration of an intermediate of the pyrimdine biosynthetic pathway suggested that this metabolite may act both as a signal for capsulation and as a cell cycle checkpoint. UDP-glucose appeared a prime candidate for this function, since it is a widely conserved signal regulating cell size and bacterial growth (VADIA AND LEVIN 2015). A transposon insertion in *galU* (encoding the enzyme required for UDP-glucose biosynthesis) prevented capsulation (GALLIE *et al.* 2015), but a role for UDP-glucose as a building block for colanic acid or as a signal for its activation remained undetermined. Introduction of a translational reporter of capsulation in the *galU* mutant (with undetectable UDP-glucose levels; GALLIE *et al.* 2015) revealed that the proportion of cells expressing this reporter was lower in the mutant compared to 1B4 (Supplementary Figure 1). This is in contrast to the predicted response if a reduction in the concentration of UDP-glucose was the signal inducing capsulation. This key result caused us to revisit the mechanistic links between pyrimidine limitation, growth rate and the heterogeneous production of colanic acid capsules.

Ribosomes are over-produced in *carB* mutants

We re-analysed transcriptomic data (published in GALLIE *et al.* 2015) to identify signalling pathways that may display different levels of activity as a result of the *carB* mutation. KEGG-enrichment analyses showed over-representation of ribosomal components among the genes that are expressed at least two-fold more in the capsulated sub-population of 1B4 (1B4 Cap+) compared to its (non-capsulated) ancestor 1A4 (Supplementary Table 1). By extracting raw expression values from the available RNAseq datasets, we observed that the average expression levels of ribosomal protein genes increase in 1B4 (either Cap- or Cap+) compared to 1A4 or SBW25 (Fig. 1a). Such a finding is surprising since ribosome production is usually proportional to growth rate (DENNIS *et al.* 2004; PAUL *et al.* 2004) and was expected to be reduced in the slower growing strain 1B4 (Supplementary Figure 2).

In bacteria, correct adjustment of ribosomal production to nutrient availability is essential to maximise growth rate. Bacteria do so by modulating transcriptional activity at the promoters of

ribosomal RNA (*rrn*) operons (DENNIS *et al.* 2004; PAUL *et al.* 2004). The production of ribosomal proteins is then adjusted to the level of available rRNA (KEENER AND NOMURA 1996). The over-expression of ribosomal protein genes in 1B4 may therefore reflect transcriptional up-regulation at *rrn* promoters. Using a chromosomally-integrated reporter, an increase in P*rrnB*-GFP transcriptional activity was detected in *carB* mutants compared to immediate ancestral types (Fig. 1b). This difference was most obvious when cultures reached OD~2, a density at which 1B4 cultures undergo a noticeable increase in capsulation (Supplementary Figure 3). Supplementing growth media with 2mM uracil – a treatment known to suppress capsulation (GALLIE *et al.* 2015) – restored wild-type P*rrnB*-GFP expression in strains carrying the mutant *carB* allele (Fig. 1b). Together with the higher total RNA concentration measured in *carB* mutants (Fig. 1c), these results show that pyrimidine limitation triggers the production of an enhanced pool of active ribosomes.

High ribosome levels are required for capsulation

The counterintuitive effect of the mutation in *carB* on ribosome levels suggested a causal connection between ribosome concentration and capsulation. In support of this hypothesis, a previous transposon-mutagenesis screen found that insertions in ribosome- or translation-associated genes (*prfC, rluB, rluC, glu/gly* tRNA) decreased or abolished capsulation in 1B4 (GALLIE *et al.* 2015). We set out to manipulate ribosome concentration in 1B4 in order to test directly if ribosome abundance has an impact on capsulation. *P. fluorescens* SBW25 harbours 5 *rrn* copies (*rrnA-E*) and, in bacteria, the deletion of a single operon can often be compensated for by the over-expression of those remaining (CONDON *et al.* 1993; BOLLENBACH *et al.* 2009; GYORFY *et al.* 2015). Capsulation was quantified in single or double *rrn* deletion mutants carrying the chromosomally-inserted translational reporter P*pflu3655*-GFP (Gallie *et al*., 2015) by measuring the proportion of GFP positive cells in cultures at the onset of stationary phase (OD~2). Whereas single mutants were not significantly affected in their capsulation levels, double mutants produced fewer capsulated cells (Fig. 2a and Supplementary Figure 4). A reduction in RNA concentration (Supplementary Figure 5) was observed in the *rrnAE* double mutant, but not in *rrnAC* that showed a milder capsulation phenotype. Together, these results show that capsulation is induced by increased ribosome dosage, which is itself a consequence of the *carB* mutation.

A ribosome-Rsm competition model for the control of capsulation

Next, we asked how ribosome abundance may influence the heterogeneous production of capsulated cells in an isogenic population. Results from a previous transposon mutagenesis screen indicated that the Gac/Rsm two-component signalling pathway is required for the production of colanic acid-like capsules (GALLIE *et al.* 2015) . The Gac/Rsm signalling pathway controls important ecological traits in many Gram-negative bacteria (VAKULSKAS *et al.* 2015; VALENTINI *et al.* 2017). Its activity is mediated through post-transcriptional regulators of the Csr/Rsm family that can prevent translation of mRNA targets by binding sites adjacent to or overlapping ribosome-binding sites (RBS) (LAPOUGE *et al.* 2008; VAKULSKAS *et al.* 2015). The phenotypic effect of the Gac/Rsm pathway was investigated by creating deletion mutants for the response regulator *gacA* and the two Csr/Rsm homologs present in SBW25, namely *rsmA* and *rsmE.* Capsulation was completely abolished in the *gacA* deletion strain, confirming the transposon-mutagenesis results (Fig. 2b). Deletion of *rsmA* or *rsmE* increased the production of capsulated cells, consistent with their typical inhibitory role in Gac/Rsm signalling pathways.

We postulated that variations in the relative concentration of free ribosomes and RsmA/E may determine translational output of a key positive regulator of capsule biosynthesis (Fig. 2c). While searching for such a regulator, attention turned to *PFLU3655*. The first gene of a putative operon (*PFLU3655-3657*) localized just upstream of the colanic acid biosynthetic operon, *PFLU3655* is annotated as a hypothetical protein carrying a two-component response regulator C-terminal domain (PFAM PF00486). *PFLU3655* is among the most highly up-regulated genes in 1B4 Cap+ cells and transposon insertions in its promoter were shown to abolish capsulation in 1B4 (GALLIE *et al.* 2015). A non-polar deletion of *PFLU3655* in 1B4 abolished capsule formation, while complementation of the mutant with an IPTG-inducible copy of *PFLU3655* on a low copy number plasmid (pME6032) restored capsulation (Fig. 3a). Over-expression of *PFLU3655* in SBW25 or 1B4 was sufficient to induce high capsulation levels in these strains, showing that PFLU3655 is a key positive regulator of colanic acid biosynthesis, the expression of which is necessary and sufficient for capsulation. Moreover, expression of PFLU3655 is also necessary and sufficient to induce the expression of its own promoter, as measured with the chromosomally-encoded P*pflu3655*-GFP translational fusion (Fig. 3b). This result shows that PFLU3655 expression can generate a positive feedback loop, a motif that can sustain bistable gene expression (VEENING *et al.* 2008; NORMAN *et al.* 2015).

Ribosome-Rsm interaction at the PFLU3655 promoter

Existence of a positive fedback loop does not warrant bistability, which often requires the additional presence of an ultrasensitive switch to convert small input deviations (typically, molecular noise) into large output differences (FERRELL AND HA 2014). When signalling components are present in large numbers, ultrasensitive responses and threshold effects can arise through molecular titration where a molecule (RNA or protein) is sequestered and inhibited by another protein (BUCHLER AND LOUIS 2008; BUCHLER AND CROSS 2009; FERRELL AND HA 2014).

The possibility that titration of a target mRNA by RsmA/E may trigger ultrasensitivity was considered. Interestingly, two putative Rsm binding sites are located in the promoter and 5' region of the coding sequence of *PFLU3655* (Fig. 4a), indicating that PFLU3655 mRNA could be a direct target of RsmA/E. The P*pflu3655*-GFP capsulation reporter was used to test this hypothesis. This translational reporter contains ~500 nucleotides upstream of PFLU3655 start codon and the first 39 coding nucleotides fused to GFP in frame; the two putative RsmA/E binding sites are conserved in this synthetic construct. Using site-directed mutagenesis, nucleotides located in the putative Rsm binding sites were substituted and effects on GFP production in the P*pflu3655*-GFP reporter determined (Fig. 4a,b). Both G-8A and A33T point mutations increased GFP production, albeit to a different extent, consistent with the expected effects arising from reduction in binding of an inhibitor. Altering the putative RBS (GG-7AC) completely abolished GFP production (Fig. 4b), which is similarly to be expected given the need for translation. Re-introducing these point mutations at the original locus in 1B4 showed that the G-8A mutation, but not the A33T, increased the proportion of capsulated cells (Fig. 4c). This difference mirrors the extent of presumed translational mis-regulation by the two point mutations and suggests that the increase in PFLU3655 translation mediated by the A33T mutation is not sufficient to increase the likelihood to jump-start the positive feedback loop, contrary to G-8A.

Together, these data support the model proposed earlier (Fig. 2c). If this model is correct, one would expect other RsmA/E targets to be over-expressed in *carB* mutants. To this end, a list of genes that were differentially expressed in a SBW25 *gacS* mutant (CHENG *et al.* 2013) was extracted and their expression levels were compared using the RNAseq dataset. On average, genes that were up-regulated in the *gacS* mutant were expressed at lower levels in 1B4 (both Cap- and Cap+) than in SBW25 or 1A4 (Supplementary Figure 6). Genes that were down-regulated in *gacS* showed a slight bias towards higher expression in 1B4 Cap+ but this difference was not statistically significant. These results are consistent with the opposing effects of *gacS* inactivation (leading to constitutive activation of RsmA/E) and *carB*-dependent increase in ribosome concentration on RsmA/E targets.

A qualitative mathematical model of the genetic network controlling bistable capsule production explains experimental results

We produced a mathematical model based on our experimental observations in order to describe the qualitative behaviour of the cells, notably the bistability of the internal state, and to predict how changes in parameters are likely to affect the fraction of capsulated cells.

The abundance of PFLU3655, represented by the variable x, is described by the following ordinary differential equation:

$$\frac{dx}{dt} = P(x) - dx$$

where P(x) is the production rate and the constant d measures the rate of degradation/dilution (or decay) per molecule. The existence of a positive feedback loop in PFLU3655 production and the plausible assumption that RsmA/E and ribosome compete to bind *PFLU3655* mRNA led us to choose an ultrasensitive curve for the production term P(x) (Fig. 5a; see Supplementary text for full details on the model), analogous to other cases of molecular titration (Buchler and Louis 2008; Buchler and Cross 2009; Zhang *et al.* 2013). For fixed concentrations of RsmA/E and ribosomes, the shape of this curve is characterized by a nonlinear increase of production with x. For low x, even though *PFLU3655* is transcribed proportionally to x, sequestration of its mRNA by RsmA/E maintains translation, thus the concentration of the protein, at low levels. When the number of mRNA molecules exceeds the buffering capacity of the RsmA/E pool, then translation increases massively, but it eventually saturates for high values of x, due to the competition for the ribosome pool.

The equilibrium solutions of the system x_E are found when the production equalizes the decay ($P(x_E)= d\ x_E$). When the decay term is sufficiently small (dashed purple line in Fig. 5a), the system is bistable, with two stable (corresponding to the OFF ($x_E=0$) and the ON ($x_E=x^{on}$) states) and one unstable ($x_E=x^S$) equilibria. The unstable solution separates the space of concentrations x in two basins of attraction of the stable equilibria. Stochastic fluctuations in the components of the system can activate or inactivate capsulation by letting x change the basin of attraction and subsequently approach the corresponding equilibrium. The smaller the basin of attraction of the OFF equilibrium, (smaller x^S) the higher the probability that random fluctuations cause the system to switch to the ON state, and vice-versa. Thus, the position of x^S defines the proportion of cells found in the capsulated ON state.

Qualitative changes in the behaviour of the system can be explored by a graphical analysis of the equilibria. An increase in ribosome concentration leads to an increase in the maximal production rate P(x), which can be sufficient to generate bistability (Fig. 5b, blue line). Starting from a bistable

situation (blue line), the probability of switching ON can be enhanced through an increase of the basal production rate of PFLU3655 (Fig. 5c**,** light blue line). These observations qualitatively match experimental results previously described (Fig. 3), indicating that this simple model encapsulates fundamental aspects of the switching mechanism.

Consequences of ribosome accumulation on growth resumption in capsulated cells

A corollary of our model is that, if ribosome levels fluctuate between isogenic cells, cells with highest ribosome concentrations should be more likely to produce capsules. Indeed, RNAseq data indicate that ribosomal protein genes are expressed at higher levels in 1B4 cap+ compared to 1B4 cap- (Fig. 1a). When the quality and/or quantity of nutrients rises abruptly, differences in ribosome abundance can be significant for bacterial fitness (MORI *et al.* 2017). Reaching higher ribosome concentration – required for maximal growth rate after nutrient up-shift – is time-consuming and means a time-delay between environment change and future growth (EHRENBERG *et al.* 2013). Cells with higher ribosome concentrations before nutrient up-shift might be considered as provisioned for rapid acclimation to the new conditions. If it is true that (i) capsulated cells have more ribosomes and (ii) ribosomes promote growth resumption after nutrient up-shift, then capsulated cells should have a fitness advantage in those conditions. To test this prediction, 1B4 cells grown to late exponential phase (OD_{600nm}~1) and cell suspensions enriched in Cap- or Cap+ cells were used to inoculate fresh cultures. The initial growth rate after nutrient up-shift in batch cultures was positively correlated with the proportion of capsulated cells (Fig. 6a). Time-lapse microscopy on solid agar pads confirmed that colonies founded by GFP+ (capsulated) cells grew approximately 10% faster than those originating from GFP- (non-capsulated) cells (Fig. 6b).

Capsulation in SBW25

The identification of mechanisms promoting the production of colanic acid capsules in evolved *P. fluorescens* genotypes raises questions as to the role and conditions for expression of colanic acid in ancestral SBW25. In bacteria, extracellular capsules are important for bacterial pathogenicity (ROBERTS 1996) and are associated with broader environmental versatility (RENDUELES *et al.* 2017). Recent work has also demonstrated a role for colanic acid-like capsules in the positioning of the cells at the surface of bacterial colonies, providing them with a better access to oxygen and a fitness advantage (KIM *et al.* 2014; KIM *et al.* 2016).

In order to test if capsulation could occur in wild-type SBW25 colonies, we spot-inoculated bacterial suspensions on agar plates and incubated the plates at 28°C for several days. Mucoid swellings were

observed from 5 days post-inoculation and increased over time (Fig. 7a). These swellings were not observed with a colanic acid mutant and their appearance was delayed when 2mM uracil was added to agar plates (Fig. 7b). In SBW25, cells sampled from mucoid regions showed a high proportion of capsulated cells, approximately 60% of which expressed the Ppflu3655-GFP reporter (Fig 7c). However, when streaked on new agar plates, no phenotypic difference was observed between cells coming from these mucoid areas and regular SBW25 colonies (data not shown), indicating that mucoidy was not dependent on *de novo* mutation. These results are in accord with predictions and indicate that capsulation in starved SBW25 colonies is also a consequence of bistable colanic acid production resulting from nutrient limitation.

Given previous results with 1B4, the possibility arose that capsulated SBW25 cells might also benefit from a growth advantage upon exposure to rich medium. Cells were collected from 7-day old colonies and enriched in capsulated or non-capsulated cells by gentle centrifugation. When transfered to fresh batch cultures, cell suspensions enriched in capsulated cells showed a faster initial growth rate (Supplementary Figure 7) that resulted in a fitness advantage during head-to-head competition (Fig. 7d). Moreover, time-lapse microscopy revealed that micro-colonies founded by GFP+ cells display an initial growth rate significantly higher than colonies arising from GFP- cells (Fig 7e).

To test if capsulation status in SBW25 is also associated with higher ribosome content, we measured expression of the ribosomal protein gene *rpsL* in capsulated and non-capsulated cells originating from old SBW25 colonies by RT-qPCR. We found an expression ratio of 1.67 (+/- 0.35 s.d., n=5, two-tailed t-test: p=0.012) in cap+ vs. cap- cells, suggesting that SBW25 capsulated cells contain more ribosomes than their non-capsulated counter-parts.

Overall, the results from experiments carried out in SBW25 are consistent with the capsulation model proposed for 1B4. During 'long-term' (*i.e.*, 7 days) starvation, nutrient limitation (possibly flux through the pyrimidine pathway and likely associated with spatial heterogeneity within colonies) establishes a sub-population of cells with increased ribosome content. This population then has an enhanced chance of flipping to the capsulated state where growth remains slow and cells enter a semi-quiescent state. This same sub-population then stands primed for rapid growth upon nutrient upshift.

Discussion:

Studies of adaptive phenotypes derived from selection experiments are by nature multifaceted, but two parallel lines of inquiry are of particular importance. The first concerns the nature of the adaptive phenotype, including its selective and molecular causes. The second concerns the ecological significance of the traits affected by adaptive evolution, prior to the occurrence of the adaptive mutation(s). A satisfactory answer to the first requires understanding of the latter.

Consider initial discovery of the 1B4 switching genotype (BEAUMONT *et al.* 2009): a remarkable behaviour that owes its existence to reduction of function of carbamoyl phosphate synthase (GALLIE *et al.* 2015). In and of itself discovery of the causal switch-generating mutation shed no light on the adpative phenotype. Understanding began to emerge upon recognition that the *carB* mutation had altered the activation threshold of a pre-existing switch.

Here we have substantially extended understanding of both the mechanistic bases of phenoytpic switching in the derived 1B4 genotype, and also the ecological significance of the underlying traits in the ancestral genotype. The former is specific to the selection experiment, whereas the latter has likely relevance of a more general nature. Indeed, as is often the case, studies of phenotypes derived from in vitro selection experiments can shed light on hitherto unrecognised aspects of bacterial physiology (HINDRE *et al.* 2012; RAINEY *et al.* 2017; and references therein).

With attention on the mechanistic basis of the 1B4 switch, experiments examining function of the switch in a *galU* mutant showed that the previous conclusions concerning the central role of UTP or related molecules required revision. While pyrimidine biosynthesis and the UTP decision point are important components of the pathways leading to capsulation, the mechanism of switching resides elsewhere. Data presented here have led to formulation of a compelling new model of the switch. Central to the proposed model (Fig. 2c) is titration of *PFLU3655* mRNA by RsmA/E that has the potential to generate an ultrasensitive response. The increase in ribosome production resulting from the *carB* mutation brings the system closer to its activation threshold, where small fluctuations in ribosome and/or in RsmA/E activities initiate a positive feedback loop leading to capsulation. Given the prevalence of inhibitory interactions in signaling networks, pathways with these features offer a common route for the evolution of or evolutionary tuning of bistable switches through relatively minor changes to the basal level (or interaction affinity) of threshold-defining components (BUCHLER AND CROSS 2009; ROTEM *et al.* 2010).

Data supporting this revised model comes largely from experiments described here, but also incorporates data presented in Gallie *et al.* (2015) that at the time were inexplicable. Most notably

data indicating a role for ribosomes, which stemmed from transcriptome data, but also from analysis of mutants defective in switching obtained from the original suppressor study. Here numerous non-switching types carried transposon insertions in genes implicated in ribosome or translation-associated activities. Additional mutants that remained unincorporated included that Gac pathway and its connection to RsmA/E and the newly recognised regulator of colanic-acid production (PFLU3655).

Understanding the switch requires understsanding of its role in the ancestral genotype. Previous work showed that switching to the capsulated type was accompanied by a reduction in growth rate. This work also showed that the probability of switching to the capsulated state was more likely in starved cells (particularly in cells starved of pyrimidines). This was understood as a mechanism that allowed cells entering starvation conditions to hedge their bets in the face of uncertainty surrounding the future state of the environment (GALLIE *et al.* 2015). Discovery (from this work) that capsulated cells, despite slow growth, are replete in ribosomes was perplexing, but caused attention to focus on exit from the semi-quiescent state. Just as cells entering a slow growing phase stand to be out-competed by conspecific types that remain in the active growth phase if the environment unexpectedly returns to one conducive for growth, cells exiting from a slow growth state stand to be out-competed by types that are already actively growing unless they can rapdily resume “life in the fast lane”.

Although the subject of little attention in the microbiological world (but see (MORI *et al.* 2017) and below), the importance of provisioning future generations with resources sufficient to aid estabishment is a central part of life-history evolution theory (STEARNS 1992). It is not difficult to conceive that cells entering a slow or non-growing state, such as persistors, or the capsulated cells of SBW25, will through evolutionary time, experience selection for mechanisms that facilitate rapid re-entry to active growth. Our data here is strongly indicative of such an evolutionary response.

Nutrient starvation leads to stochastic activation of capsulation and entry into a semi-quiescent growth phase. At the same time such capsulated cells contain above average concentrations of ribosomes. Upon encountering conditions conducive for growth capsulated cells rapidly switch to the non-capsulated state (GALLIE *et al.* 2015), but remarkably, out-compete non-capsulated cells. A phenomenom of ribosome over-capacity that bears similarity to what we have interpreted as ‘ribosome provisioning’, was described previously in fast growing bacteria (KOCH 1971): production of excess ribosomes during exponential growth, while being deleterious in the short term, can provide an advantage during nutrient up-shift (MORI *et al.* 2017). In environments where resource availability fluctuates, it appears that the control of ribosome biosynthesis might be subjected to a

trade-off between maximising growth rate before starvation and growth resumption upon nutrient up-shift (MORI *et al.* 2017). Our findings add a single-cell perspective showing that cell-to-cell heterogeneity in ribosome activity during stationary phase may contribute to maximisation of long-term geometric mean fitness.

Material and methods:

Bacterial strains and growth conditions

Bacterial strains used in this study are listed in Supplementary Table 2. Unless otherwise stated, *Pseudomonas fluorescens* strains were cultivated in King's Medium B (KB; KING *et al.* 1954)) at 28°C with orbital shaking. *Escherichia coli* DH5α λ*pir* was used for clonings and was grown on Lysogeny Broth at 37°C. Bacteria were plated on their respective growth medium containing 1.5% agar. Antibiotics were used at the following concentrations: ampicillin (50-100 µg mL^{-1}), gentamicin (10 µg mL^{-1}), tetracycline (10 µg mL^{-1}), kanamycin (25 or 50 µg mL^{-1} for *E. coli* or *P. fluorescens*, respectively) and nitrofuorantoin (100 µg mL^{-1}). Uracil (Sigma-Aldrich) was added to culture medium at 2mM final concentration when indicated. For competition experiments, 5-bromo-4-chloro-3-indolyl-β -d-galactopyranoside (X-gal) was used at a concentration of 60 mg L^{-1} in agar plates.

For capsulation assays, pre-cultures were inoculated from pre-calibrated dilutions of frozen glycerol aliquots in order to reach an optical density of 0.3-0.5 after overnight culture.

For colony assays with SBW25, 5µl of cell suspensions were spot-inoculated on KB agar plates and incubated for 7 days at 28°C. Cells from the center of these colonies were resuspended in PBS or Ringer's solution for growth and competition assays and time-lapse microscopy, or in RNAlater solution (Invitrogen) for RT-qPCR.

Molecular techniques

Oligonucleotides and plasmids used in this study are listed in Supplementary Tables 3 and 4, respectively. Standard molecular biology techniques were used for DNA manipulations (SAMBROOK *et al.* 1989). DNA fragments used to generate promoter fusions and gene deletion constructs were prepared by splicing by overhang extension polymerase chain reaction (SOE-PCR; HO *et al.* 1989). All

DNA fragments generated by SOE-PCR were first cloned into the pGEM-T easy vector (Promega) and their fidelity was verified by Sanger sequencing (Macrogen, Seoul, South-Korea). Plasmids were introduced into *P. fluorescens* by tri-parental conjugations with the helper plasmid pRK2013, carrying the *tra* and *mob* genes required for conjugation. Tn7-based plasmids were mobilized into recipient strains with the additional helper plasmid pUX-BF13 (BAO *et al.* 1991).

To generate deletion mutants (*rrn* operons, *gacA, rsmA, rsmE* and *pflu3655*), regions flanking the genes or operons of interest were amplified from SBW25 genomic DNA and assembled by SOE-PCR. Deletion cassettes were inserted into the pUIC3 plasmid (RAINEY 1999) as SpeI fragments and mutants were obtained following the two-step allelic exchange protocol described previously (ZHANG AND RAINEY 2007). Deletion mutants were checked by PCR. To check *rrn* copy number after *rrn* deletions, quantitative PCR were performed using a protocol described previously (FARR *et al.* 2017).

For complementation and over-expression studies, *PFLU3655* was amplified with oPR206/oPR207 and cloned into pME6032 (HEEB *et al.* 2002) as *EcoR*I/*Xho*I restriction fragment, downstream of the P*tac* promoter.

To generate the Tn7-P*rrnB*-GFP reporter, a ~600bp fragment upstream of the *rrnB* operon (*PFLUr7-11*) was amplified from SBW25 genomic DNA (oPR148/oPR151) and fused by SOE-PCR to *gfp-mut3.1* sequence containing the T0 terminator previously amplified with oPR152/FluomarkerP2 from the miniTn7(Gm)-P*rrnB1-gfp-a* plasmid (Lambertsen *et al.* 2003). The resulting fragment was cloned into pUC18R6K-miniTn7T-Gm (CHOI *et al.* 2005) as a *Spe*I restriction fragment.

Site-directed mutagenesis of putative RsmA/E binding sites in pGEMTeasy-P*pflu3655*-GFP plasmid was performed using the Quick Change mutagenesis kit (Stratagene) according to manufacturer's instructions. Mutagenized fragments were then cloned into pUC18R6K-miniTn7T-Gm (CHOI *et al.* 2005) as a *Spe*I restriction fragment. In order to re-engineer point mutations in RsmA/E into *Pseudomonas fluorescens* genome, a 1.5kb fragment spanning equal length on each site of the target sites was amplified with oPR37/oPR223 and cloned into pGEM-T easy vector. Site-directed mutagenesis was performed on this plasmid as described above, and the resulting DNA fragments were cloned in pUIC3 as *Spe*I restriction fragments and introduced into *P. fluorescens* genome by double recombination.

RNA extractions and RT-qPCR

For quantification of RNA concentration in bacterial cultures, cells were harvested from 1ml of cultures at OD 0.5-1 and resuspended in 200ul of RNAlater solution (Invitrogen). For total RNA

quantification, we followed the method described by You *et al.* (2013), except that, before processing, cells cultures were resuspended in RNAlater (Invitrogen) instead of being fast frozen on dry ice. To normalise total RNA concentrations, the relationship between cell density and OD_{600nm} was established for each strain by counting cells with a hemocytometer in 5 independent cultures of similar OD to those used for RNA extractions.

Reverse-transcription quantitative PCR were performed as described previously (FARR *et al.* 2017), using *gyrA* as an internal control. Oligonucleotide primers used for RT-qPCR are listed in Supplementary Table 3.

Capsulation and gene expression assays

For capsulation test, cells were grown from standardized glycerol aliquots stored at -80°C. Aliquots were diluted in KB and pre-cultures were grown overnight in order to reach an OD ~0.3-0.5 in the morning. For gene expression studies, overnight pre-cultures were grown to saturation. In both cases, pre-cultures were diluted to OD_{600nm}=0.05 in KB and incubated at 28°C. IPTG was added to a final concentration of 0.1-1mM when indicated. Samples were taken at different time points for flow cytometry and OD measurements. GFP fluorescence in bacterial populations was measured with a BD FACS Canto II flow cytometer. Cell suspensions were diluted to a density of ~ 10^5 cells ml^{-1} in filter-sterilised PBS and at least 20,000 cells were analysed by flow cytometry. Cellular debris were filtered using side- and forward-scatter channels. GFP fluorescence was detected with a 488 nm laser with 530/30 bandwidth filter. Laser intensity was set to 600V, except for P*rrnB*-GFP analyses where intensity was lowered to 300V. Flow cytometry data files were analysed in R using the flowCore package (ELLIS *et al.* 2017).

Growth curves in microplate reader

Overnight precultures were adjusted to OD_{600nm}=0.05 in fresh KB and used to start growth curves in a Synergy 2 microplate reader (Biotek) in 96-well plates. Cultures were incubated for at least 24h at 28C with constant shaking and OD_{600nm} was read every 5 minutes.

To measure growth rates of cultures enriched in capsulated or non-capsulated cells, cells were harvested from late-exponential phase (OD_{600nm}~1; 1B4) or 7-day old colonies (SBW25) and centrifuged (1 min, 3000 rpm). Supernatants and pellets were collected, representing sub-populations enriched in capsulated and non-capsulated cells, respectively. Cell suspension density

453 was adjusted to OD_{600nm}=0.05 in KB to start growth curves. Initial growth rates were calculated by
454 performing a linear regression on the logarithm of the measure OD values during the first 2h of
455 growth. Slopes of these linear regressions are reported as growth rate values.

456

457 *Microscopy*

458 Indian ink staining of capsulated cells was performed as described previously (GALLIE *et al.* 2015). For
459 time-lapse microscopy, bacteria were harvested from late exponential phase (1B4, OD~1-2) or from
460 7 day-old colonies (SBW25), diluted 1:1000 in KB and 2µl of the resulting suspension was
461 immediately transferred on a gel pad (1% agar KB) located on a glass slide within an adhesive frame
462 (GeneFrame, Thermo-Fisher). When dry, a cross-section of the pad was removed with a razor blade
463 in order to allow gaz exchanges to occur, the preparation was sealed with a glass cover-slip and
464 transferred to the microscope incubation chamber pre-heated at 28°C. Time lapse microscopy
465 experiments was performed with an Olympus BX61 upright microscope equipped with an F-View II
466 monochrome camera, a motorized stage and a temperature-controlled chamber set at 28°C. Devices
467 were operated by the Olympus Cell^P or CellSens softwares. Phase-contrast images were acquired
468 every 10 minutes with an oil-immersion 100x objective. One GFP image was taken before starting
469 the experiment in order to determine the capsulation status of each cell.

470 Phase contrast images were segmented with Fiji (SCHINDELIN *et al.* 2012) and individual colony areas
471 were extracted. For each colony analysed, the capsulation status of founding cell was scored
472 manually. The logarithm of the growth rate of individual 1B4 colonies was then fitted using a linear
473 regression. For SBW25, segmented linear regressions were found to better fit the data and the slope
474 of the first line was reported.

475

476 *RNAseq analyses*

477 RNAseq data were published previously (GALLIE *et al.* 2015). KEGG orthology terms for SBW25
478 genome were downloaded from the KEGG Orthology database (www.genome.jp; accessed in April
479 2016). KEGG enrichment statistics were computed with a hypergeometric test and was performed
480 separately for up- and down-regulated genes. Data from the transcriptome analysis of gacS mutant
481 were retrieved from supplementary table 3 in Cheng *et al.* (2013).

482

483 *Competition experiments*

SBW25 or SBW25-*lacZ* cell suspensions were spot-inoculated on separate KB agar plates and grown for 7 days. Cells from the central ring were harvested, resuspended in Ringer's solution and gently centrifuged to enrich suspensions in capsulated or non-capsulated cells. Capsulated SBW25 cells were mixed with non-capsulated SBW-*lacZ* cells, and vice-versa. Mixed suspensions were diluted 100x in fresh KB and grown at 28°C in shaken tubes for 4h. Appropriate dilutions of the cultures were plated on KB + X-gal plates at 0, 2h and 4h post-inoculation in order to measure the ratio of white-blue colonies.

Acknowledgements:

The authors thank H. Hendrickson and P. Lind for help with microscopy and flow cytometry, respectively, XX. Zhang for the generous gift of pUIC3-Δ*gacA* deletion plasmid, and E. Denisenko for assistance with KEGG enrichment analyses. This work was supported in part by the Marsden Fund Council and a James Cook Research Fellowship from government funding administered by the Royal Society of New Zealand.

Supplementary text: description of the mathematical model

The protein PFLU3655 is a key regulator for capsulation; we assume that the amount of colanic acid (and fluorescence from the P*pflu3655-GFP* reporter) produced by the cell is proportional to PFLU3655 concentration, described by the variable *x*. The rate of change of *x* will be the result of production, at rate P(x), and of degradation and dilution, whose rates can be for simplicity assumed proportional to x. The time change of x will thus be described by the following ordinary differential equation:

$$\frac{dx}{dt} = P(x) - dx$$

where the constant d measures the rate of degradation/dilution (or decay). The equilibrium solutions of the system x_E are such that the production equalizes the decay, that is when $P(x_E) = d\, x_E$. We can constrain the shape of the production P(x) term based on the experimental results. PFLU3655 generates a positive feedback loop, meaning that P(x) is a positive function and the production of the corresponding mRNA will be increasing with x (the more PFLU3655 protein, the higher the production of mRNA). If there was no post-trancriptional regulation, the amount of mRNA would determine the amount of protein produced, and P(x) would follow a Michealis-Menten kinetics whose saturation value would be set by the concentration R of ribosomes (the higher the concentration of ribosomes, the higher the maximal amount of protein that can be produced). In this case, the system would be monostable and cells would be either on or off ($x_E=0$ or $x_E=x^{on}$), depending on whether the baseline production is smaller or larger than the decay, respectively.

When protein production is regulated post-transcriptionally, however, the competition of RsmA/E and ribosomes (whose concentrations are assumed to be constant) for binding to the mRNA can produce an ultrasensitive dependence of P(x) on x (Fig. 5a; black line). For small x, the produced *PFLU3655* mRNA will be almost entirely sequestered by RsmA/E and translation will be prevented. Above a threshold concentration x_T, the titration by RsmA/E will be no longer sufficient to prevent PFLU3655 proteins being produced, so that the production will be positive (but maybe insufficient to overcome the decay term). If the affinity of RsmA/E is much stronger than that of ribosomes, the shape of P(x) will be very nonlinear, with the production term being effectively zero for $x<x_T$. Finally, for high x we expect production to saturate because of the finite amount of available ribosomes.

It is well known that ultrasensitivity can produce bistability (MUKHERJI *et al.* 2011; ZHANG *et al.* 2013; FERRELL AND HA 2014). This is graphically illustrated in Fig. 5a: when the decay term (the slope of the dashed red line) is sufficiently small, there will be three equilibrium solutions. Two of these solutions are stable, corresponding to the OFF ($x_E=0$) and the ON ($x_E=x^{on}$) states, and one unstable ($x_E=x^S$). The

unstable solution separates the space of concentrations x in two domains: for all $x<x^S$, the concentration will decrease and eventually approach the OFF state, for larger concentrations it will converge to the ON state. The position of x^S, thus the extension of the basins of attraction of the two stable equilibria, determines what is the probability that random fluctuations in the protein concentration or in its production will lead the system to change equilibrium. For instance, the probability to switch ON will be higher the smaller the value of x^S.

To examine what qualitative changes in the state of the system are expected following a variation in its parameters, let us first imagine that for the WT strain in exponential phase of growth the decay line lays just above the production curve (Fig. 5a; solid red line): cells will be almost exclusively in the OFF state, even though rare large fluctuations in the protein concentration may lead them to be 'trapped' for some time in the region around the ON state. In the *carB* mutants, an increase in ribosome concentration leads to an increase in the maximal production rate such that the two curves cross in three points (Fig. 5b). There are now two alternative stable states, and the population will contain a sizeable fraction of capsulated cells.

Changes in the parameters of the system can lead both to the transition from mono- to bistability and to a change in the extent of the basins of attraction of the two stable equilibria, thus of the population composition. When the baseline level of protein production is increased, as for instance when the gene *PFLU3655* is inserted on a plasmid (Fig. 3b), the curve P(x) is displaced towards higher values (Fig. 5c). This causes both the threshold concentration (thus the proportion of ON cells) and the protein concentration (thus cell fluorescence) to increase.

553 **References:**

554 Ackermann, M., 2015 A functional perspective on phenotypic heterogeneity in microorganisms. Nat
555 Rev Microbiol 13**:** 497-508.
556 Bao, Y., D. P. Lies, H. Fu and G. P. Roberts, 1991 An improved Tn7-based system for the single-copy
557 insertion of cloned genes into chromosomes of gram-negative bacteria. Gene 109**:** 167-168.
558 Beaumont, H. J. E., J. Gallie, C. Kost, G. C. Ferguson and P. B. Rainey, 2009 Experimental evolution of
559 bet hedging. Nature 462**:** 90-U97.
560 Bodi, Z., Z. Farkas, D. Nevozhay, D. Kalapis, V. Lazar *et al.*, 2017 Phenotypic heterogeneity promotes
561 adaptive evolution. PLoS Biol 15**:** e2000644.
562 Bollenbach, T., S. Quan, R. Chait and R. Kishony, 2009 Nonoptimal microbial response to antibiotics
563 underlies suppressive drug interactions. Cell 139**:** 707-718.
564 Buchler, N. E., and F. R. Cross, 2009 Protein sequestration generates a flexible ultrasensitive
565 response in a genetic network. Mol Syst Biol 5**:** 272.
566 Buchler, N. E., and M. Louis, 2008 Molecular titration and ultrasensitivity in regulatory networks. J
567 Mol Biol 384**:** 1106-1119.
568 Cheng, X., I. de Bruijn, M. van der Voort, J. E. Loper and J. M. Raaijmakers, 2013 The Gac regulon of
569 Pseudomonas fluorescens SBW25. Environ Microbiol Rep 5**:** 608-619.
570 Choi, K. H., J. B. Gaynor, K. G. White, C. Lopez, C. M. Bosio *et al.*, 2005 A Tn7-based broad-range
571 bacterial cloning and expression system. Nat Methods 2**:** 443-448.
572 Condon, C., S. French, C. Squires and C. L. Squires, 1993 Depletion of functional ribosomal RNA
573 operons in Escherichia coli causes increased expression of the remaining intact copies.
574 EMBO J 12**:** 4305-4315.
575 Dennis, P. P., M. Ehrenberg and H. Bremer, 2004 Control of rRNA synthesis in Escherichia coli: a
576 systems biology approach. Microbiol Mol Biol Rev 68**:** 639-668.
577 Ehrenberg, M., H. Bremer and P. P. Dennis, 2013 Medium-dependent control of the bacterial growth
578 rate. Biochimie 95**:** 643-658.
579 Ellis, B., P. Haaland, F. Hahne, N. Le Meur, N. Gopalakrishnan *et al.*, 2017 flowCore: Basic structures
580 for flow cytometry data, R package version 1.44.0.
581 Farr, A. D., P. Remigi and P. B. Rainey, 2017 Adaptive evolution by spontaneous domain fusion and
582 protein relocalization. Nat Ecol Evol 1**:** 1562-1568.
583 Ferrell, J. E., Jr., and S. H. Ha, 2014 Ultrasensitivity part II: multisite phosphorylation, stoichiometric
584 inhibitors, and positive feedback. Trends Biochem Sci 39**:** 556-569.
585 Fridman, O., A. Goldberg, I. Ronin, N. Shoresh and N. Q. Balaban, 2014 Optimization of lag time
586 underlies antibiotic tolerance in evolved bacterial populations. Nature 513**:** 418-421.
587 Gallie, J., E. Libby, F. Bertels, P. Remigi, C. B. Jendresen *et al.*, 2015 Bistability in a metabolic network
588 underpins the de novo evolution of colony switching in Pseudomonas fluorescens. PLoS Biol
589 13**:** e1002109.
590 Gyorfy, Z., G. Draskovits, V. Vernyik, F. F. Blattner, T. Gaal *et al.*, 2015 Engineered ribosomal RNA
591 operon copy-number variants of E. coli reveal the evolutionary trade-offs shaping rRNA
592 operon number. Nucleic Acids Res 43**:** 1783-1794.
593 Heeb, S., C. Blumer and D. Haas, 2002 Regulatory RNA as mediator in GacA/RsmA-dependent global
594 control of exoproduct formation in Pseudomonas fluorescens CHA0. J Bacteriol 184**:** 1046-
595 1056.
596 Hindre, T., C. Knibbe, G. Beslon and D. Schneider, 2012 New insights into bacterial adaptation
597 through in vivo and in silico experimental evolution. Nat Rev Microbiol 10**:** 352-365.
598 Ho, S. N., H. D. Hunt, R. M. Horton, J. K. Pullen and L. R. Pease, 1989 Site-directed mutagenesis by
599 overlap extension using the polymerase chain reaction. Gene 77**:** 51-59.
600 Keener, J., and M. Nomura, 1996 Regulation of ribosome synthesis, pp. 1417-1431 in *Escherichia coli*
601 *and Salmonella: cellular and molecular biology*, edited by F. C. Neidhardt, R. Curtiss III, J. L.
602 Ingraham, E. C. C. Lin, K. B. Low *et al.* American Society for Microbiology, Washington, D.C.

603 Kim, W., S. B. Levy and K. R. Foster, 2016 Rapid radiation in bacteria leads to a division of labour. Nat
604 Commun 7: 10508.
605 Kim, W., F. Racimo, J. Schluter, S. B. Levy and K. R. Foster, 2014 Importance of positioning for
606 microbial evolution. Proc Natl Acad Sci U S A 111: E1639-1647.
607 King, E. O., M. K. Ward and D. E. Raney, 1954 Two simple media for the demonstration of pyocyanin
608 and fluorescin. J Lab Clin Med 44: 301-307.
609 Koch, A. L., 1971 The adaptive responses of Escherichia coli to a feast and famine existence. Adv
610 Microb Physiol 6: 147-217.
611 Lapouge, K., M. Schubert, F. H. Allain and D. Haas, 2008 Gac/Rsm signal transduction pathway of
612 gamma-proteobacteria: from RNA recognition to regulation of social behaviour. Mol
613 Microbiol 67: 241-253.
614 Mori, M., S. Schink, D. W. Erickson, U. Gerland and T. Hwa, 2017 Quantifying the benefit of a
615 proteome reserve in fluctuating environments. Nat Commun 8: 1225.
616 Mukherji, S., M. S. Ebert, G. X. Zheng, J. S. Tsang, P. A. Sharp *et al.*, 2011 MicroRNAs can generate
617 thresholds in target gene expression. Nat Genet 43: 854-859.
618 New, A. M., B. Cerulus, S. K. Govers, G. Perez-Samper, B. Zhu *et al.*, 2014 Different levels of
619 catabolite repression optimize growth in stable and variable environments. PLoS Biol 12:
620 e1001764.
621 Norman, T. M., N. D. Lord, J. Paulsson and R. Losick, 2015 Stochastic Switching of Cell Fate in
622 Microbes. Annu Rev Microbiol 69: 381-403.
623 Paul, B. J., W. Ross, T. Gaal and R. L. Gourse, 2004 rRNA transcription in Escherichia coli. Annu Rev
624 Genet 38: 749-770.
625 Rainey, P. B., 1999 Adaptation of Pseudomonas fluorescens to the plant rhizosphere. Environ
626 Microbiol 1: 243-257.
627 Rainey, P. B., P. Remigi, A. D. Farr and P. A. Lind, 2017 Darwin was right: where now for experimental
628 evolution? Curr Opin Genet Dev 47: 102-109.
629 Rendueles, O., M. Garcia-Garcera, B. Neron, M. Touchon and E. P. C. Rocha, 2017 Abundance and co-
630 occurrence of extracellular capsules increase environmental breadth: Implications for the
631 emergence of pathogens. PLoS Pathog 13: e1006525.
632 Richard, M., and G. Yvert, 2014 How does evolution tune biological noise? Front Genet 5: 374.
633 Roberts, I. S., 1996 The biochemistry and genetics of capsular polysaccharide production in bacteria.
634 Annu Rev Microbiol 50: 285-315.
635 Rotem, E., A. Loinger, I. Ronin, I. Levin-Reisman, C. Gabay *et al.*, 2010 Regulation of phenotypic
636 variability by a threshold-based mechanism underlies bacterial persistence. Proc Natl Acad
637 Sci U S A 107: 12541-12546.
638 Sambrook, J., E. F. Fritsch and T. Maniatis, 1989 *Molecular cloning: a laboratory manual*. Cold Spring
639 Harbor Laboratory, Cold Spring Harbor, N.Y.
640 Schindelin, J., I. Arganda-Carreras, E. Frise, V. Kaynig, M. Longair *et al.*, 2012 Fiji: an open-source
641 platform for biological-image analysis. Nat Methods 9: 676-682.
642 Stearns, S. C., 1992 *The evolution of life histories*. Oxford University Press, Oxford ; New York.
643 Vadia, S., and P. A. Levin, 2015 Growth rate and cell size: a re-examination of the growth law. Curr
644 Opin Microbiol 24: 96-103.
645 Vakulskas, C. A., A. H. Potts, P. Babitzke, B. M. Ahmer and T. Romeo, 2015 Regulation of bacterial
646 virulence by Csr (Rsm) systems. Microbiol Mol Biol Rev 79: 193-224.
647 Valentini, M., D. Gonzalez, D. A. Mavridou and A. Filloux, 2017 Lifestyle transitions and adaptive
648 pathogenesis of Pseudomonas aeruginosa. Curr Opin Microbiol 41: 15-20.
649 van Boxtel, C., J. H. van Heerden, N. Nordholt, P. Schmidt and F. J. Bruggeman, 2017 Taking chances
650 and making mistakes: non-genetic phenotypic heterogeneity and its consequences for
651 surviving in dynamic environments. J R Soc Interface 14.

652 Van den Bergh, B., J. E. Michiels, T. Wenseleers, E. M. Windels, P. V. Boer *et al.*, 2016 Frequency of
653 antibiotic application drives rapid evolutionary adaptation of Escherichia coli persistence.
654 Nat Microbiol 1**:** 16020.
655 Veening, J. W., W. K. Smits and O. P. Kuipers, 2008 Bistability, epigenetics, and bet-hedging in
656 bacteria. Annu Rev Microbiol 62**:** 193-210.
657 Zhang, Q., S. Bhattacharya and M. E. Andersen, 2013 Ultrasensitive response motifs: basic amplifiers
658 in molecular signalling networks. Open Biol 3**:** 130031.
659 Zhang, X. X., and P. B. Rainey, 2007 Construction and validation of a neutrally-marked strain of
660 Pseudomonas fluorescens SBW25. J Microbiol Methods 71**:** 78-81.

661

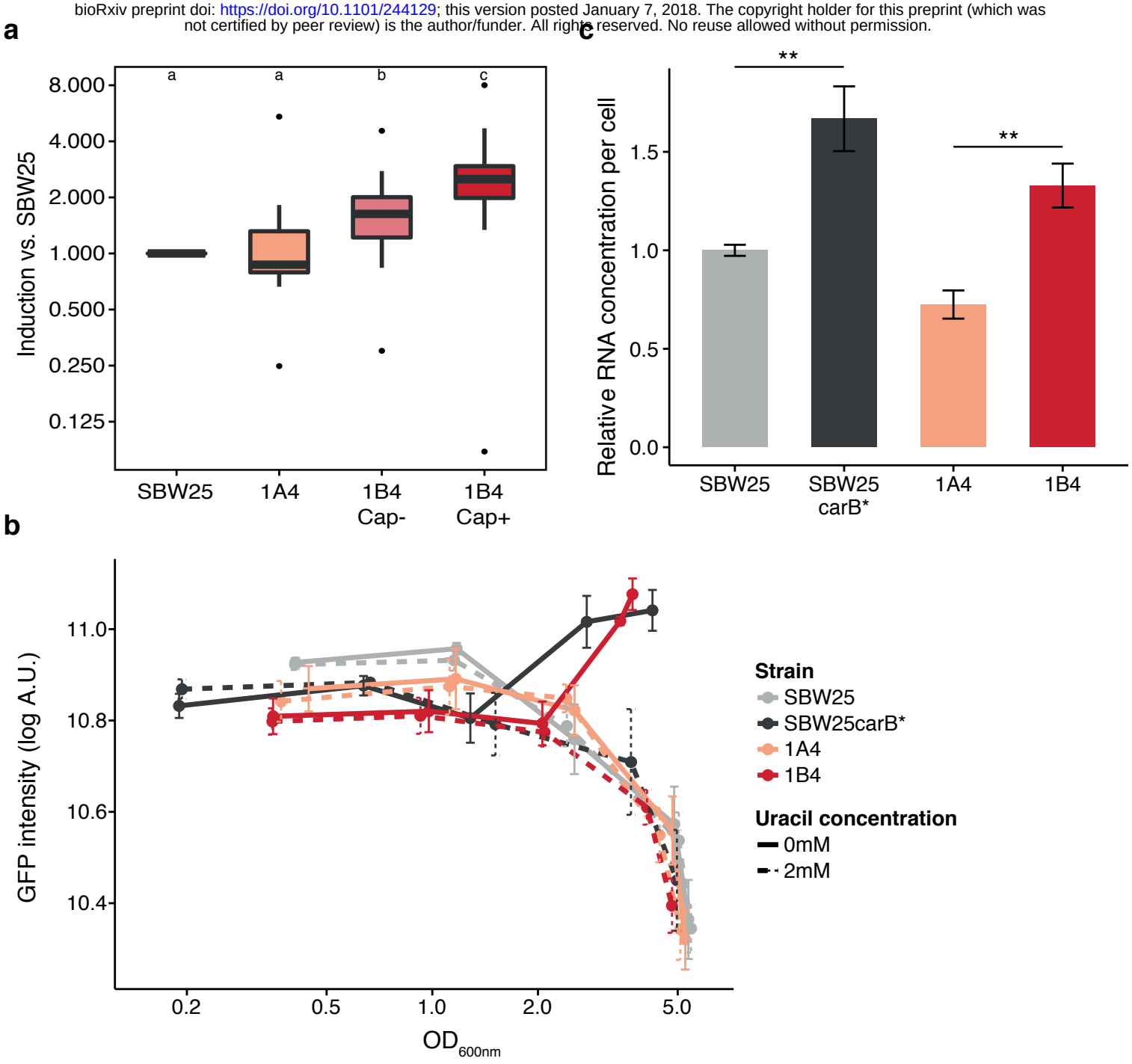

Figure 1: Increased ribosome production in *carB* mutants

a. Transcriptional induction of ribosomal protein genes in SBW25, 1A4, 1B4 Cap- and 1B4 Cap+ cells. Absolute expression levels of ribosomal protein genes (KEGG pathway '0310-Ribosomes', n=26) were extracted from a previous RNA-seq dataset (Gallie *et al.* 2015) and normalised to SBW25. Letter groups indicate statistical significance; $P < 0.05$, Kruskall-Wallis test with Dunn's post-hoc correction.

b. Expression kinetics of the P*rrnB*-GFP transcriptional reporter. Fluorescence in individual cells was measured by flow cytometry. Mean fluorescence values of bacterial populations are reported. Means ± standard deviation are shown, n=4. Data are representative of 3 independent experiments.

c. Total RNA concentration in bacterial cells during exponential phase (OD=0.5-0.6) normalized per cell count. Values were normalized to SBW25 control within each experiment. Means ± standard deviation are shown, n=6. ** $P<0.01$, Student's t-test.

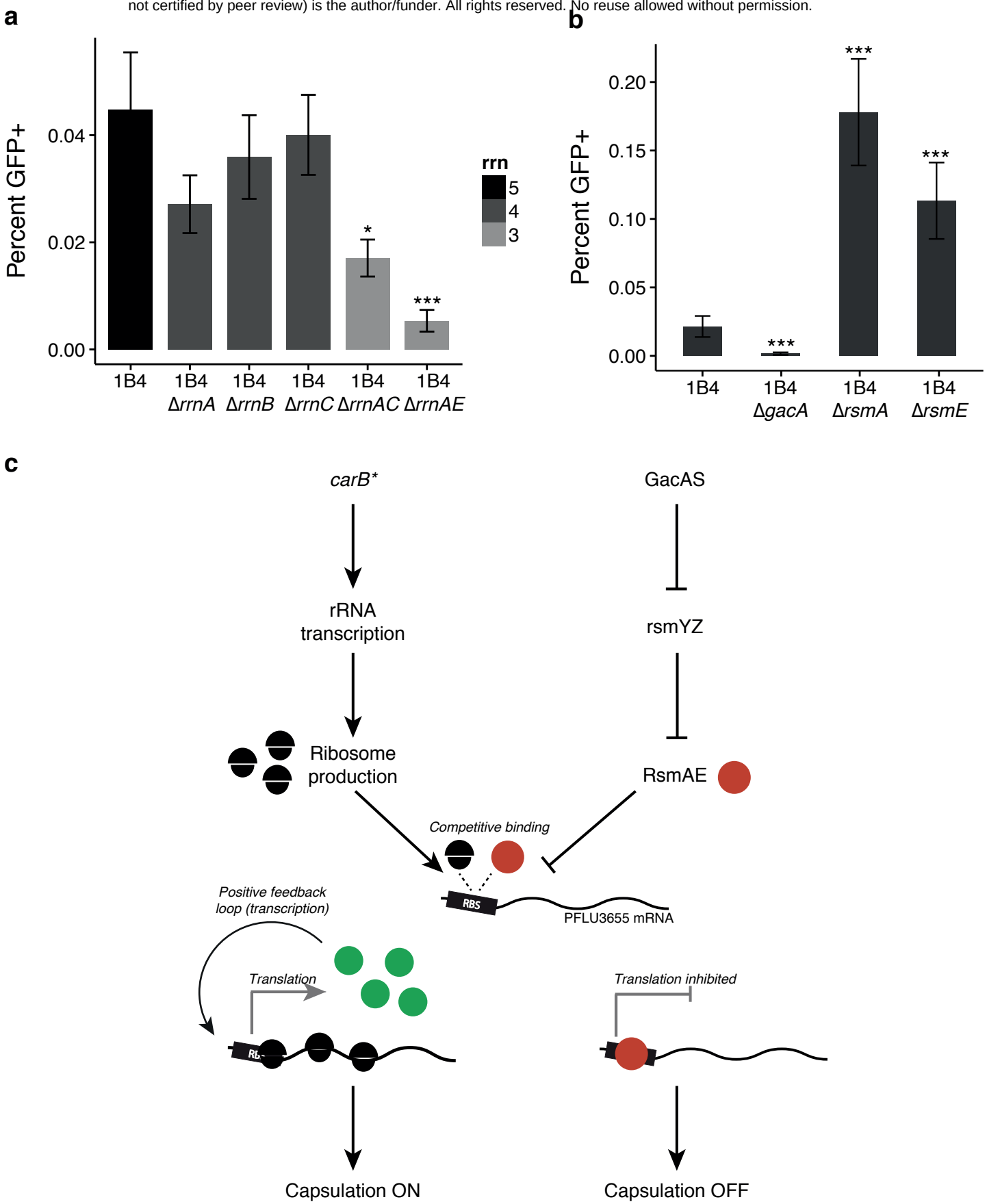

Figure 2: Genetic bases of capsulation

a. Capsulation in *rrn* deletion mutants.The Tn7-P*pflu3655*-GFP reporter was introduced in 1B4 bacteria ("WT") and its derived *rrn* mutants. Capsulation was measured by quantifying the proportion of GFP positive cells by flow cytometry at the onset of stationary phase (OD~2). Means ± standard error of the mean are shown, n≥8. Data were pooled from 4 independent experiments.* $P < 0.05$, *** $P < 0.001$, Dunn's test with Benjamini-Hochberg post-hoc correction, comparison to WT.

b. Capsulation in *gac*/*rsm* mutants. Means ± standard error of the mean are shown, n=9. Data are pooled from 3 independent experiments. *** $P < 0.001$, Dunnett's multiple comparison test on log-transformed data.

c. A model for capsulation in 1B4. See text for details.

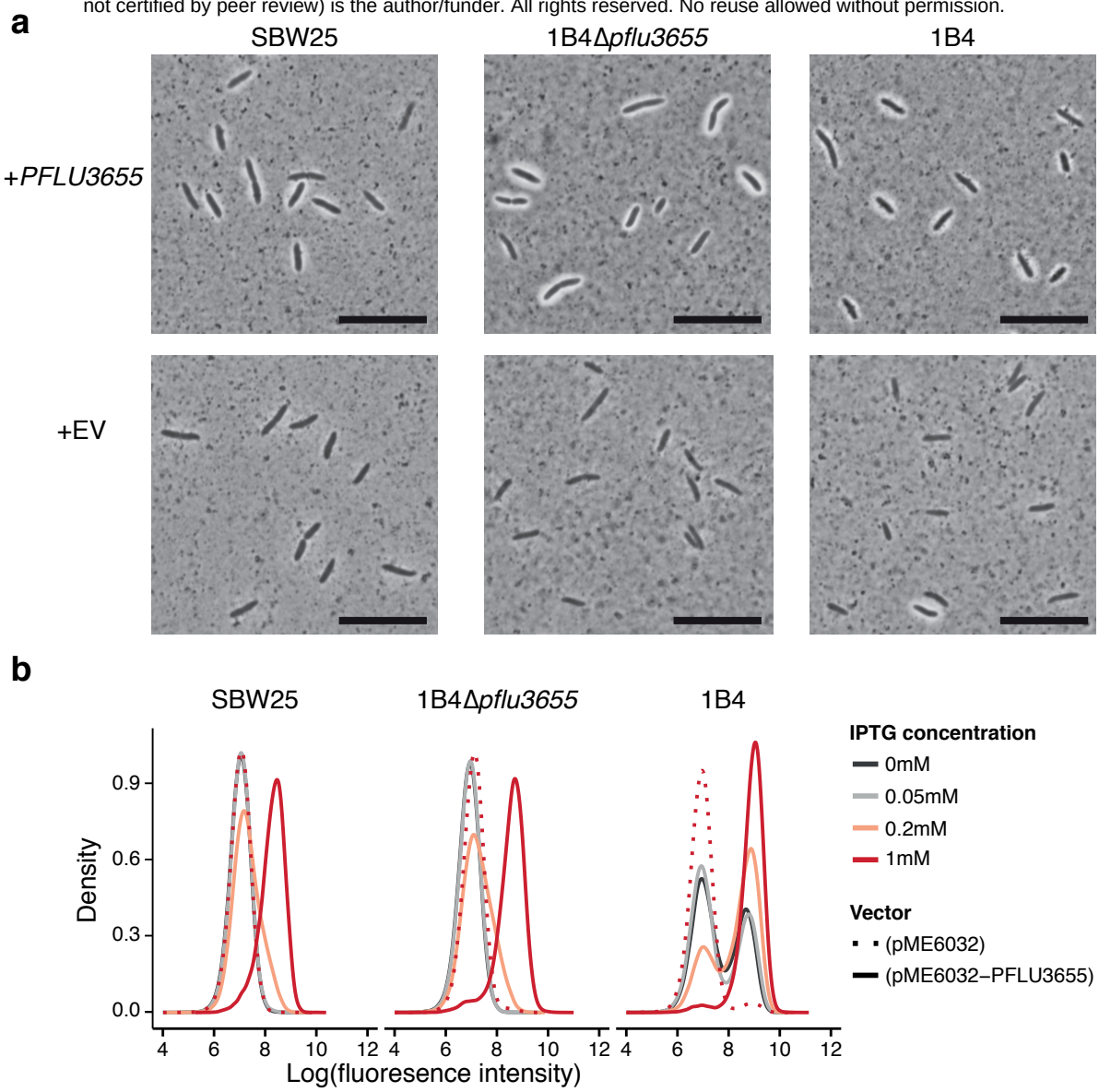

Figure 3: *PFLU3655* expression is necessary and sufficient for capsulation

a. Capsulation in SBW25, 1B4Δ*pflu3655* and 1B4 strains carrying the pME6032-*PFLU3655* plasmid or empty vector (EV) after induction with 1mM IPTG. Phase contrast microscopy images of bacterial suspensions counter-stained with indian ink. White halo around cells indicate capsulation. Scale bar = 10 µm.

b. PFLU3655 establishes a positive feedback loop. GFP fluorescence from the P*pflu3655*-GFP reporter in SBW25 (left), 1B4Δ*pflu3655* (middle) or 1B4 (right) cells carrying the pME6032-*PFLU3655* plasmid or empty vector. *PFLU3655* expression was induced with IPTG at indicated concentration and fluorescence was measured by flow cytometry. Smoothed fluorescence distributions are shown. Data are representative of 3 independent experiments.

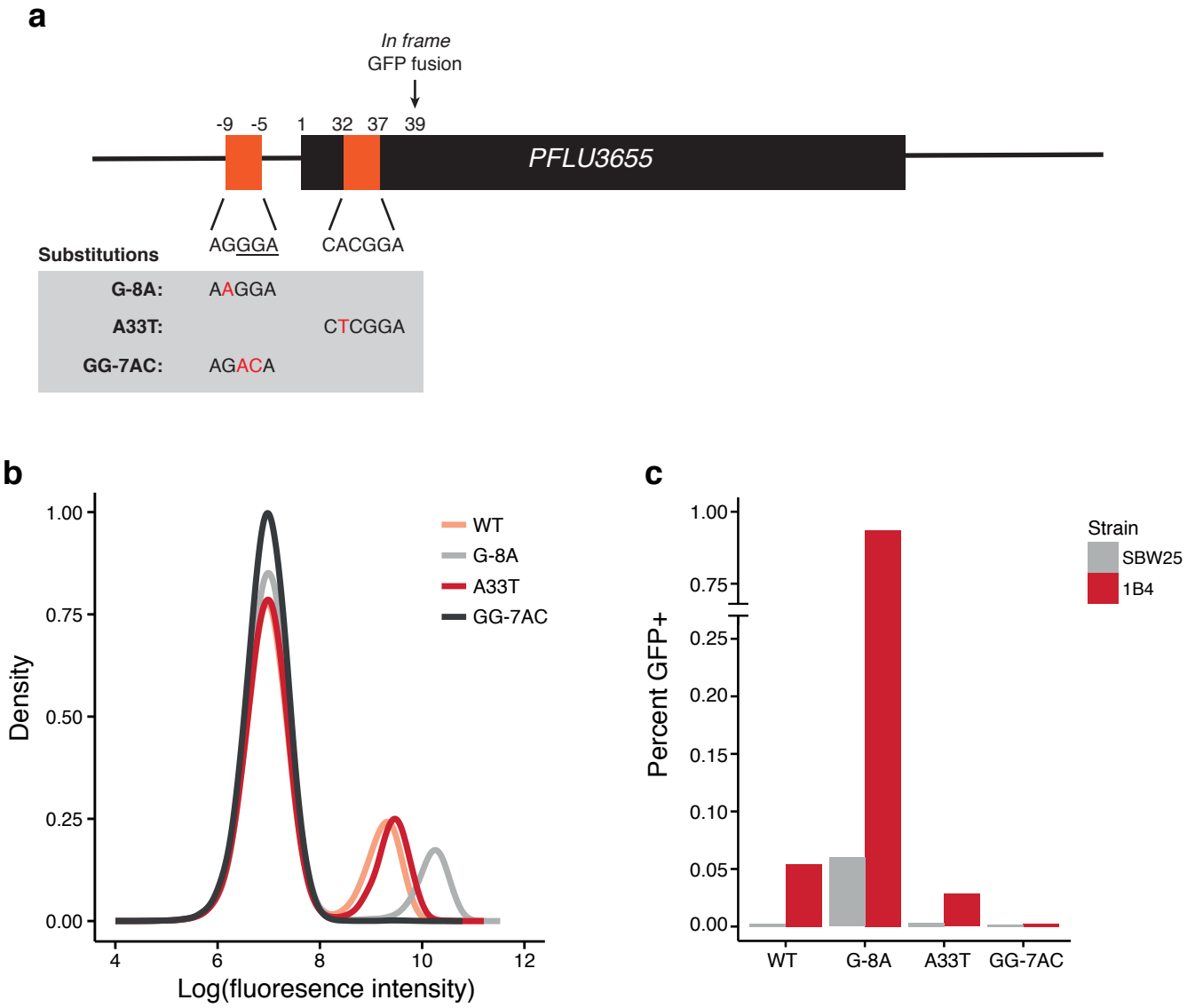

Figure 4: *PFLU3655* is a direct target of RsmA/E

a. Schematic diagram of *PFLU3655* region. Two putative RsmA/E binding sites (orange squares) are located in the promoter and 5' region of the gene. Numbers indicate nucleotide position relative to start codon (not to scale). Sequences of putative RsmA/E binding sites are shown, the putative ribosome-binding site (RBS) is underlined. Below: point mutations introduced in the different sequences by site-directed mutagenesis.

b. Expression of the P*pflu3655*-GFP reporter carrying the different point mutations in the 1B4 background. GFP fluorescence was measured by flow cytometry, smoothed distributions are shown. Data are representative of 3 independent experiments.

c. Mutations in putative RsmA/E binding sites affect capsulation. Individual point mutations were re-introduced into SBW25 and 1B4 carrying the wild-type P*pflu3655*-GFP reporter and the proportion of GFP positive cells in late exponential phase (OD~1-2) was measured by flow-cytometry.

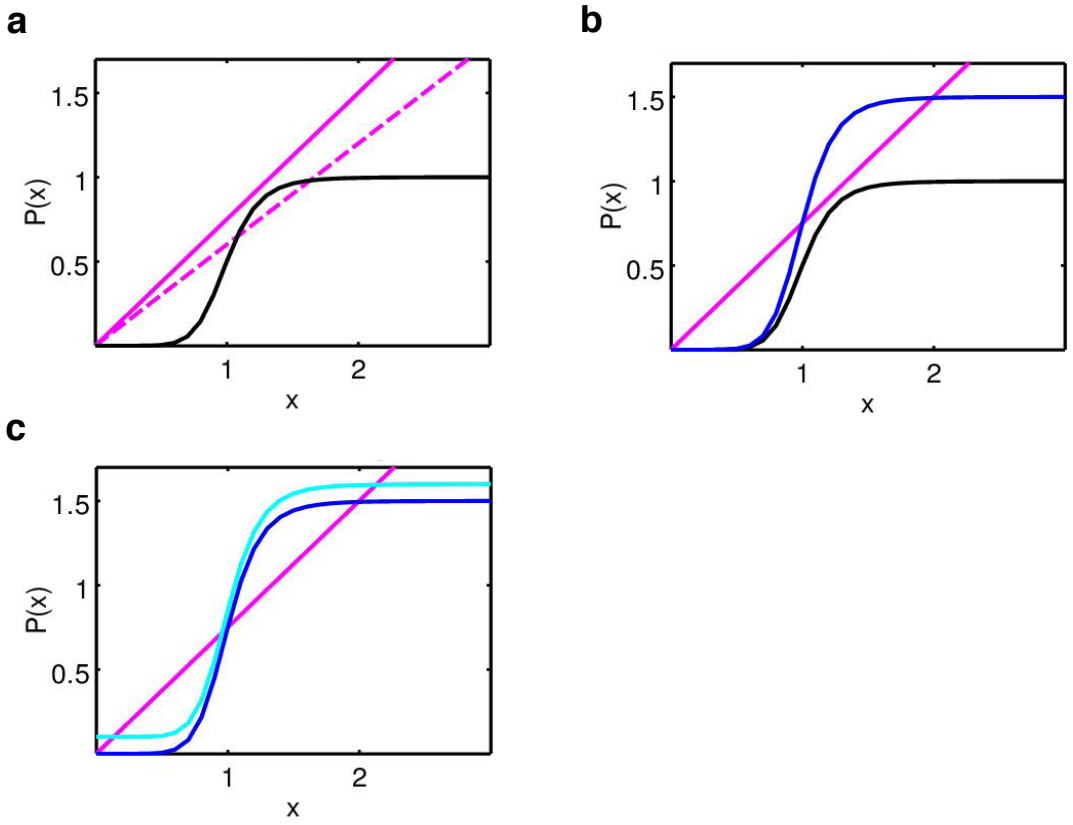

Figure 5: A mathematical model of capsulation allows to qualitatively explain switching behaviour

Graphical analysis of the effect of parameters on switching behaviour. Growth rate (a), ribosome concentration (b) and basal transcription rate of *PFLU3655* (c) can all affect the position of the equilibrium points.

Production curves P(x) are represented in black for wild-type SBW25 (a,b), in blue for *carB* mutants (b,c), and light blue for *carB* mutants with increased basal transcription of *PFLU3655* (c). Decay curves are drawn in purple. Stable or unstable equilibria are located at the intersections between production and decay curves.

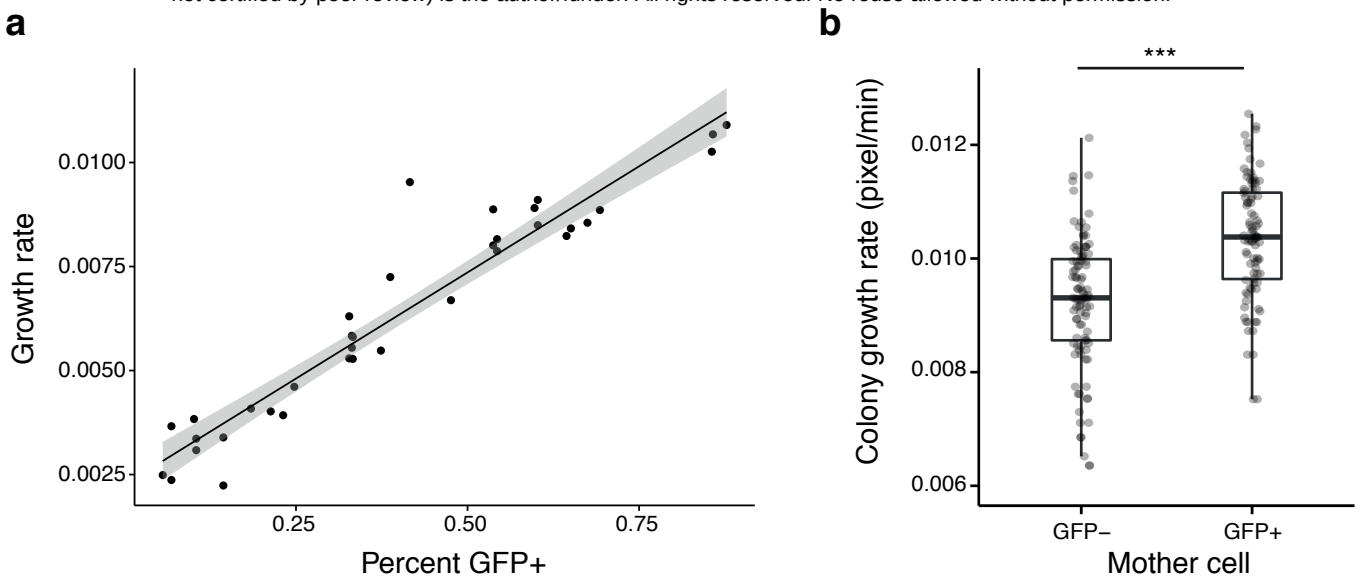

Figure 6: Capsulation and growth in 1B4

a. Initial growth rate after nutrient upshift depends on the proportion of capsulated cells in 1B4 populations. Data points pooled from 2 independent experiments. n=36, r^2=0.91. Shaded area indicates 95% confidence interval.

b. Growth rate of micro-colonies founded by cap- (GFP-) or cap+ (GFP+) cells measured by time-lapse microscopy. Growth rate was measured as the coefficient of the linear fit of the logarithm of colony area over time during the first 2h of growth. n=97 for GFP-; n=94 for GFP +. *** $P < 0.001$, Wilcoxon test.

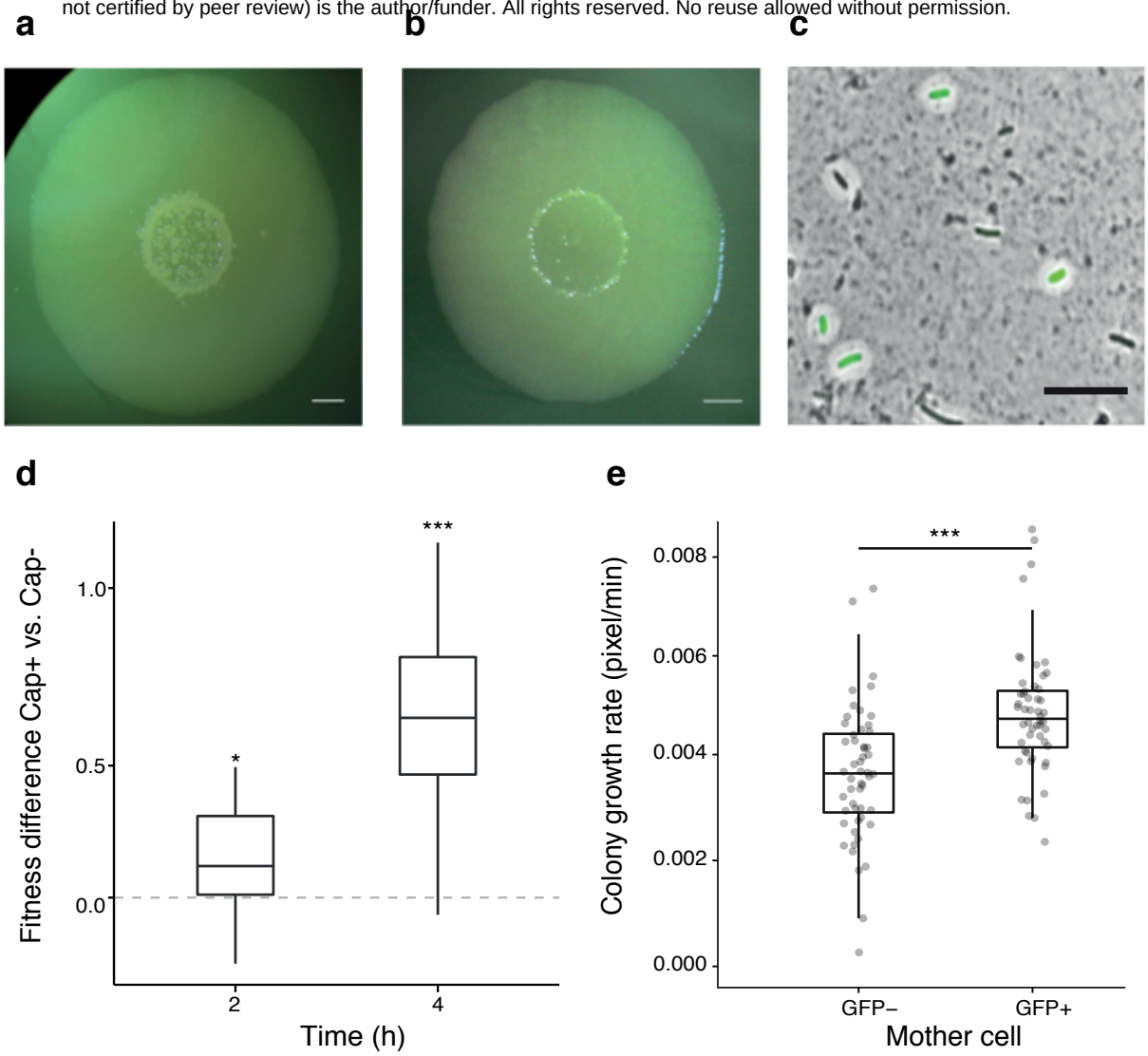

Figure 7: Capsulation and growth in SBW25

a-b. SBW25 colony grown on KB agar plate (a) or KB agar plate supplemented with 2mM uracil (b) for 7 days. Scale bar = 2 mm.

c. SBW25 cells carrying the Tn7-P*pflu3655*-GFP reporter and sampled from a 7-days old colony were counter-strained with indian ink to detect the presence of colanic-acid capsules. GFP images are overlaid to the phase contrast image. Scale bar = 10 µm.

d. Competitive fitness difference between SBW25 Cap- and Cap+ cells. Boxplot of he differences in Malthusian parameters between cultures enriched in Cap+ vs. Cap- cells are shown, n=12. * $P<0.05$, *** $P<0.001$, comparison to 0 with Student's t-test.

e. Growth rate of microcolonies founded by GFP- or GFP+ cells measured by time-lapse microscopy. Growth rate was measured as the first coefficient from the segmented fit of the logarithm of colony area over time during the first 2h of growth. n=65. *** $P < 0.001$, Wilcoxon test.

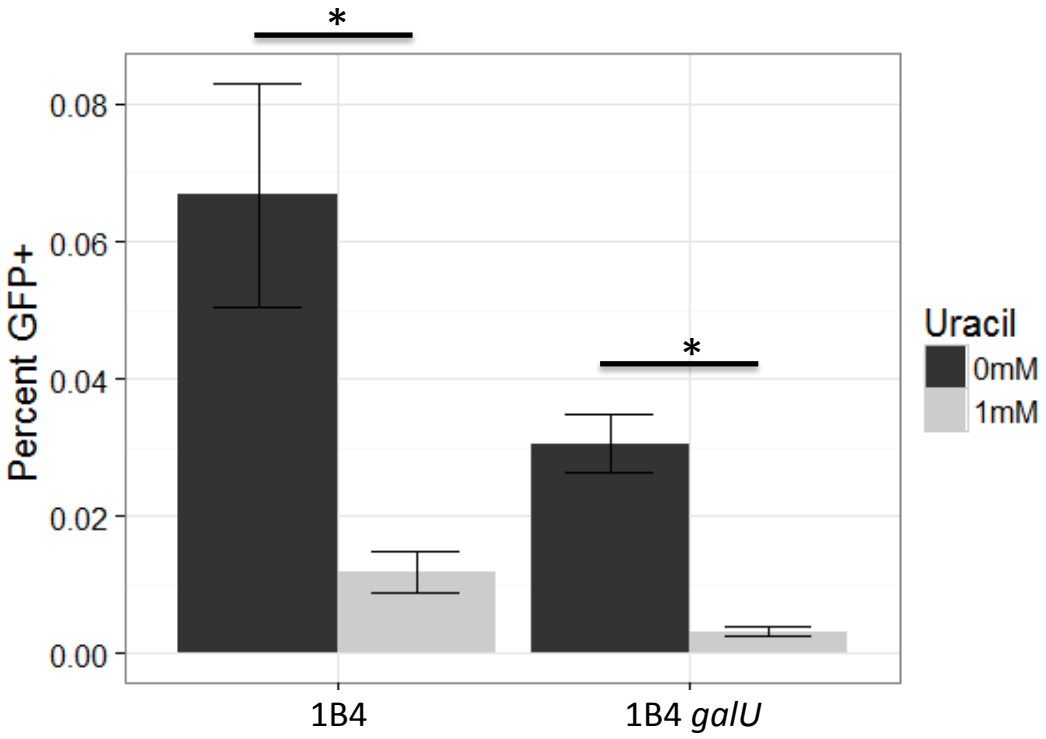

Supplementary Figure 1: Capsulation in the *galU* mutant

The Tn7-P*pflu3655*-GFP reporter was introduced in 1B4 and *galU* mutant. Capsulation was measured by quantifying the proportion of GFP positive cells by flow cytometry at the onset of stationary phase. Means ± standard deviation are shown. * $P < 0.05$, Student's t-test, n = 12.

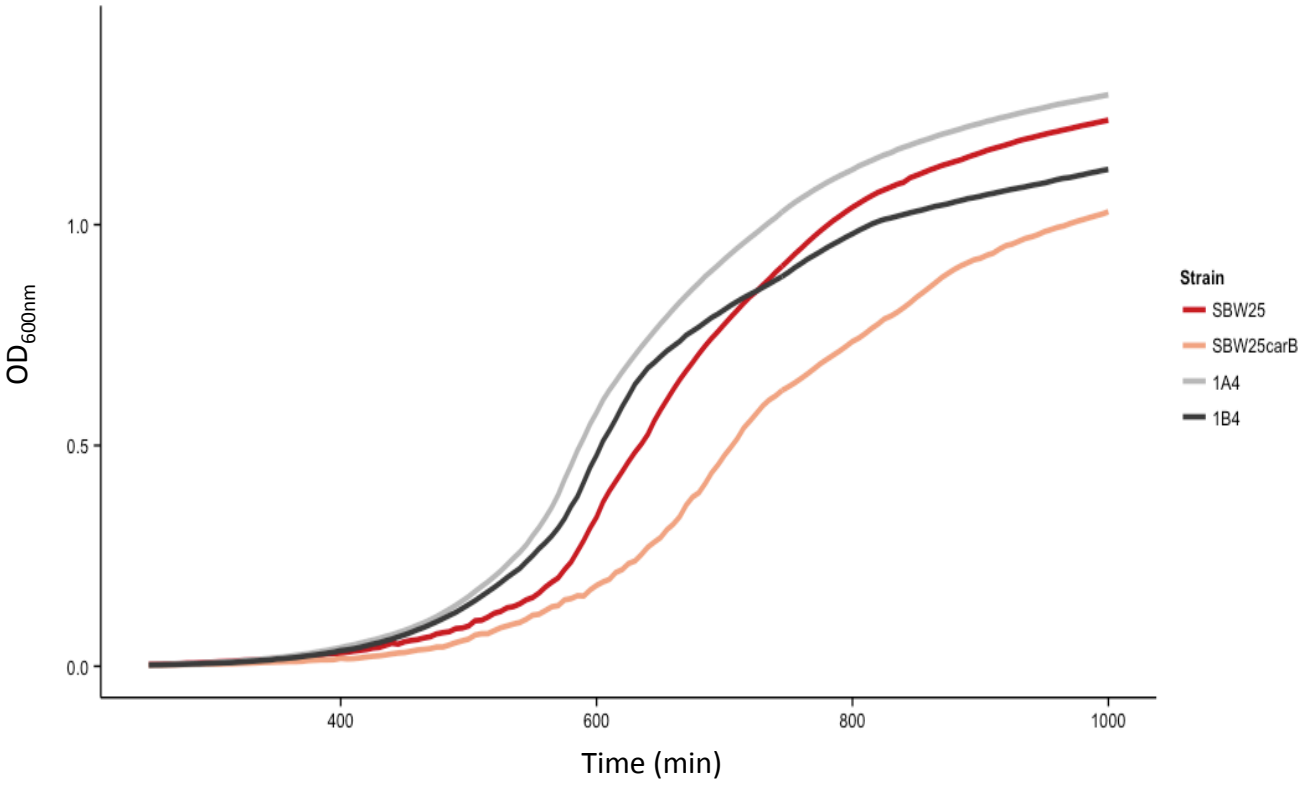

Supplementary Figure 2: Growth curves of *carB* mutants

Growth kinetics of SBW25, SBW25 *carB*, 1A4 and 1B4 strains in KB medium. Overnight cultures were diluted and used to inoculate 200µl KB cultures in a 96-well plate. OD_{600nm} was read in a microplate reader every 5min during incubation at 28°C with continuous shaking. Lines represent mean from 3 technical replicates.

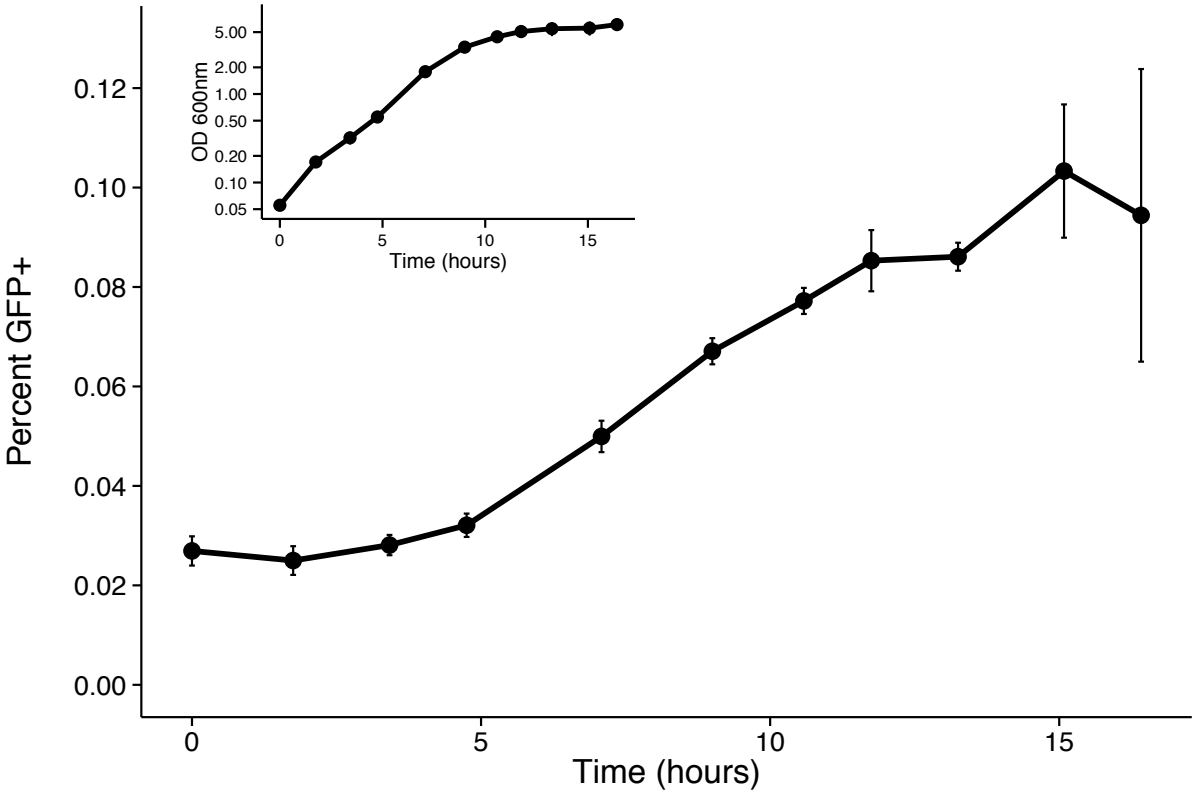

Supplementary figure 3: Capsulation kinetics in 1B4

The Tn7-P*pflu3655*-GFP reporter was introduced in 1B4. OD_{600nm} (inset) and the size of GFP positive subpopulation (main panel) were monitored over >15h. Capsulation was measured by quantifying the proportion of GFP positive cells by flow cytometry. Means ± standard deviation are shown, n=3. Data are representative of 2 independent experiments.

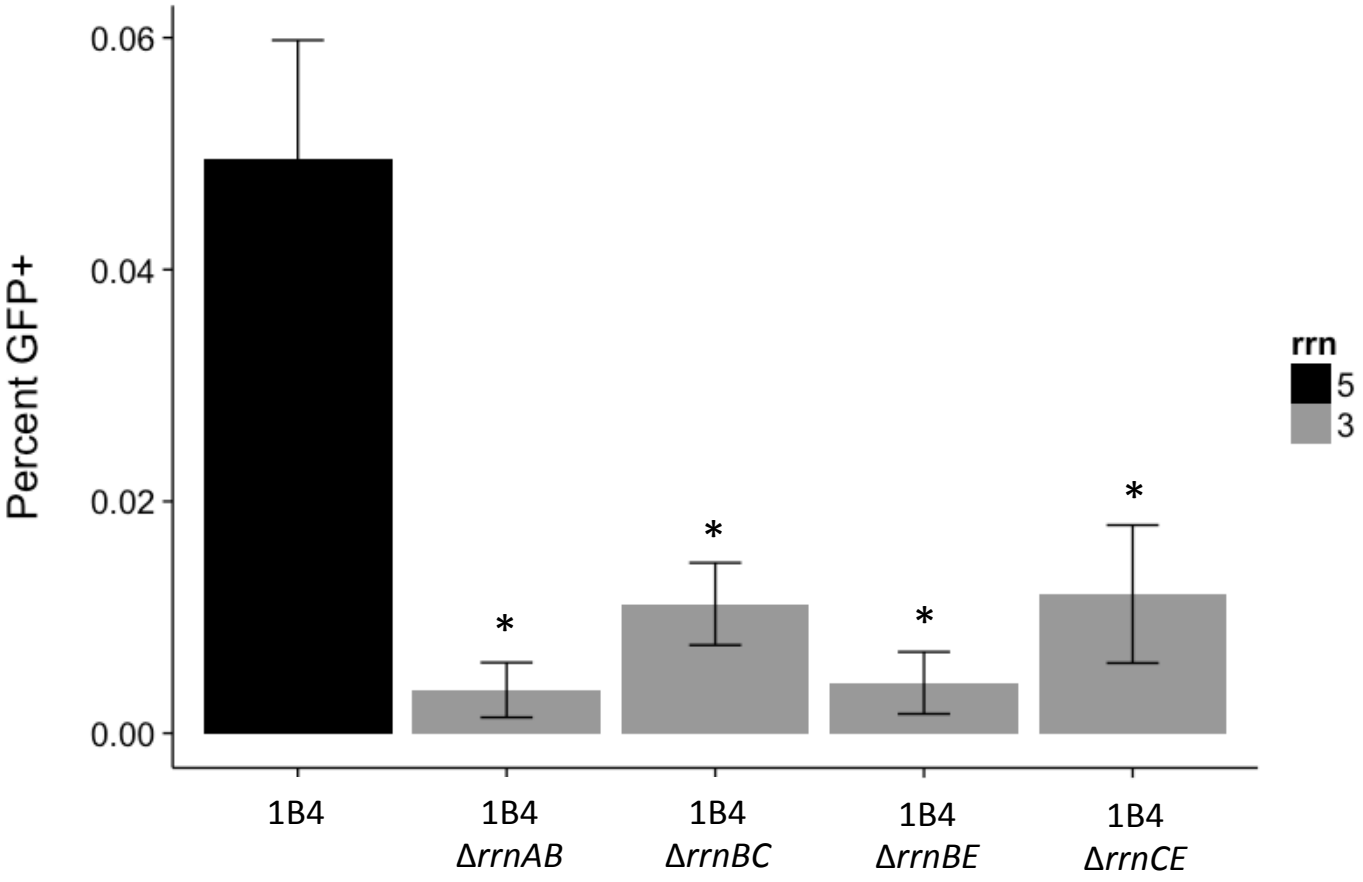

Supplementary Figure 4: Capsulation frequency in double *rrn* mutants
The Tn7-Pp*flu3655*-GFP reporter was introduced in 1B1 bacteria ("WT") and its derived *rrn* mutants. Capsulation was measured by quantifying the proportion of GFP positive cells by flow cytometry at the onset of stationary phase (OD~2). Color indicate the number of *rrn* operons per genotype. Means and standard error of the mean are shown, n≥9. Data are pooled from 3 independent experiments. * $P < 0.05$ compared to WT, Dunn's test with Benjamini-Hochberg post-hoc correction.

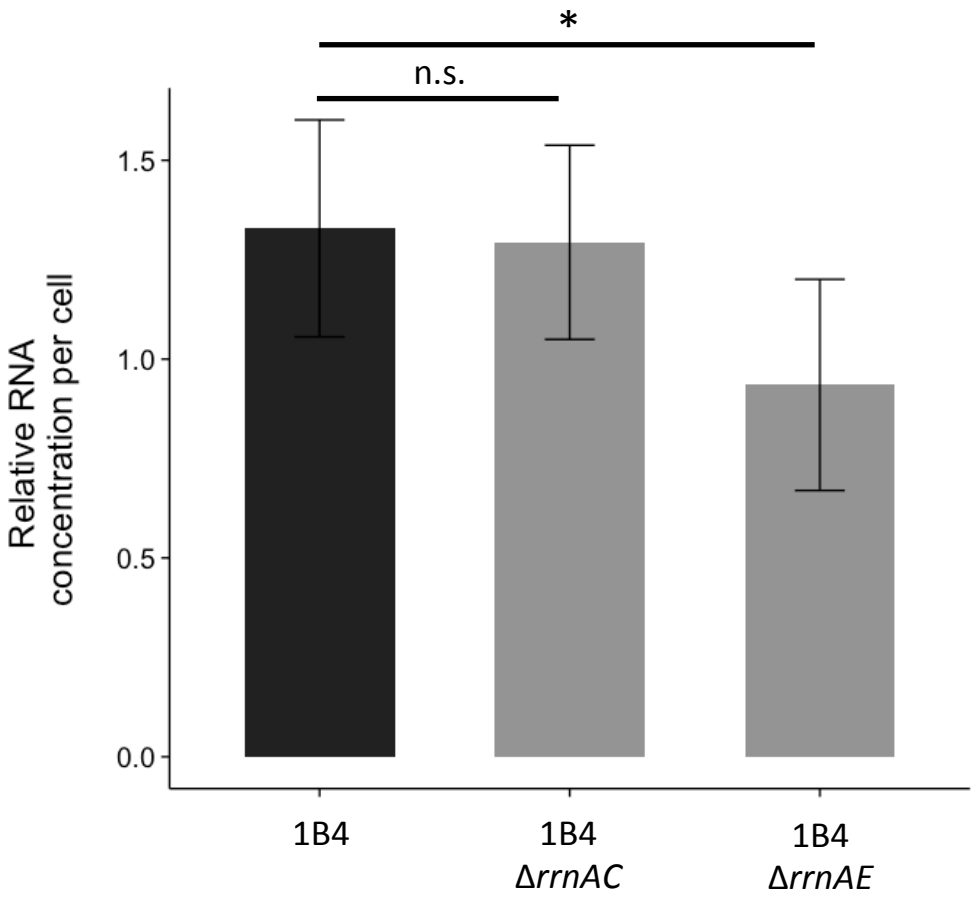

Supplementary Figure 5: RNA quantification in *rrn* mutants
Total RNA concentration in bacterial cells during exponential phase (OD=0.5-0.6) normalized per cell count. Values were normalized to SBW25 control within each experiment. Means ± standard deviation are shown, n=6. * *P*<0.05, Student's t-test. n.s. = not signifcant.

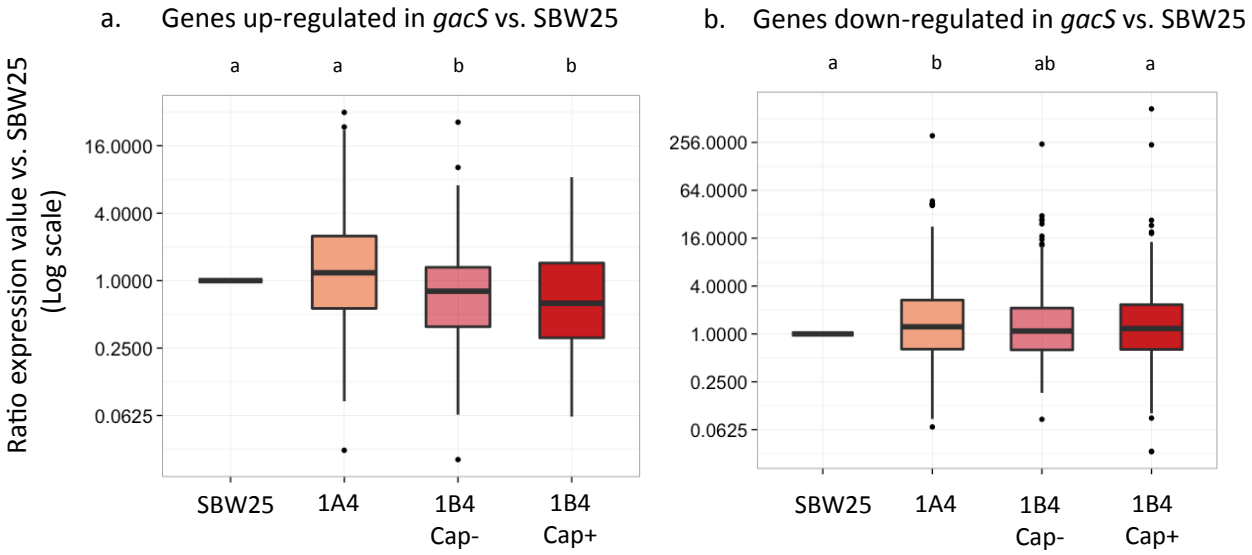

Supplementary figure 6: Expression of *gacS*-regulated genes

Genes that are up-regulated (left) or down-regulated (right) more than 4 times in a *gacS* mutant compared to WT SBW25 were recovered from Cheng *et al.* 2013 (dataset from supplementary table 3). The distribution of induction or repression values (after normalization by the base expression in SBW25) in the different RNAseq datasets is shown for each set of genes. n=125 (a) or 165 (b). Letter groups indicate statistical significance at $P < 0.05$, Kruskall-Wallis test with Dunn's post-hoc correction.

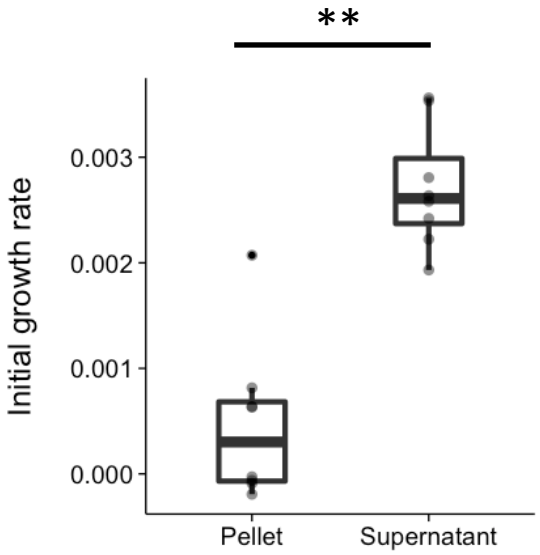

Supplementary Figure 7: Growth rate of SBW25 cultures enriched in Cap- or Cap+ cells

Cells from 7-day old colonies were resuspended in KB medium and suspensions were enriched in Cap- (pellet) or Cap+ (supernatant) cells by gentle centrifugation. The growth of these suspensions in a 96-well plate was measured with a microplate reader and the slopes from the fit of logarithm of density increase over time during the first 2h of growth are shown. n=8. ** $P < 0.01$, Wilcoxon test.